The Astrophysical Journal, 921:45 (9pp), 2021 November 1 https://doi.org/10.3847/1538-4357/ac1c7b

The IceCube Pie Chart: Relative Source Contributions to the Cosmic Neutrino Flux

I. Bartos[1], D. Veske[2], M. Kowalski[3,4,5], Z. Márka[5], and S. Márka[2]
[1] Department of Physics, University of Florida, PO Box 118440, Gainesville, FL 32611-8440, USA; imrebartos@ufl.edu
[2] Department of Physics, Columbia University, New York, NY 10027, USA
[3] Deutsches Elektronen Synchrotron DESY, Platanenallee 6, D-15738 Zeuthen, Germany
[4] Institut fur Physik, Humboldt-Universit at zu Berlin, D-12489 Berlin, Germany
[5] Columbia Astrophysics Laboratory, Columbia University, New York, NY 10027, USA
Received 2021 May 8; revised 2021 August 6; accepted 2021 August 8; published 2021 October 29

Abstract

Neutrino events from IceCube have recently been associated with multiple astrophysical sources. Interestingly, these likely detections represent three distinct astrophysical source types: active galactic nuclei (AGNs), blazars, and tidal disruption events (TDEs). Here, we compute the expected contributions of AGNs, blazars, and TDEs to the overall cosmic neutrino flux detected by IceCube based on the associated events, IceCube's sensitivity, and the source types' astrophysical properties. We find that, despite being the most commonly identified sources, blazars cannot contribute more than 11% of the total flux (90% credible level), consistent with existing limits from stacked searches. On the other hand, we find that either AGNs or TDEs could contribute more than 50% of the total flux (90% credible level), although stacked searches further limit the TDE contribution to $\lesssim$30%. We also find that so-far unknown source types contribute at least 10% of the total cosmic flux with a probability of 80%. We assemble a pie chart that shows the most likely fractional contribution of each source type to IceCube's total neutrino flux.

Unified Astronomy Thesaurus concepts: Cosmological neutrinos (338); Neutrino astronomy (1100)

1. Introduction

The universe produces a quasi-diffuse flux of high-energy (>TeV) neutrinos (hereafter cosmic neutrino flux; Aartsen et al. 2013, 2014), whose properties are now well-characterized (Aartsen et al. 2016). The origin of this cosmic flux is, nevertheless, not yet understood.

High-energy neutrinos have recently been identified from several distinct astrophysical sites. These sources include the TXS 0506+056 blazar (Aartsen et al. 2018a, 2018b), a nearby Seyfert galaxy (NGC 1068; Aartsen et al. 2020c), and a tidal disruption event (TDE; AT2019dsg; Stein et al. 2021). Several other blazars have also been identified with probable high-energy neutrino associations (Kadler et al. 2016; Kun et al. 2021). At the same time, the contribution of several source types to the overall flux have been constrained, including blazars (Yuan et al. 2020), TDEs (Murase & Waxman 2016; Senno et al. 2017; Guépin et al. 2018; Stein 2019; Murase et al. 2020b), and gamma-ray bursts (GRBs; Abbasi et al. 2012).

In this paper, we evaluate the expected overall contribution of different source types to the cosmic neutrino flux based on the associated *individual* neutrino sources, taking into account the uncertainty in source associations. We show that the widely differing properties of different source types mean that the same number of detections translates to different expected contributions to the overall flux. In addition, computing the expected contribution of each source type to the overall cosmic neutrino flux allows us to estimate the fraction of the overall flux that arrives from so-far unidentified source types, i.e., sources that are not active galactic nuclei (AGNs), blazars, or TDEs.

An additional goal of the present description is to demonstrate how different source features, such as their number density, number of detections, or their cosmic rate evolution, contribute to their estimated contribution to the overall neutrino flux. Therefore, before discussing our full Bayesian estimate, we first derive simpler estimates in which the role of different source properties is more accessible.

The paper is organized as follows. We first carry out our simplest "warm-up" calculation of fractional contributions in Section 2 using detections that followed high-energy neutrino alerts publicly released by IceCube. Next, we introduce a simplified model in Section 3 that highlights the relative importance of population properties. We then introduce our most detailed and realistic method in Section 4, and in Section 5 we discuss its implementation to obtain the estimated relative contributions for both detected and unknown source types. Results for this most detailed model are presented in Section 6. We summarize our conclusions in Section 8.

2. Warming up: the Fraction of Discoveries

It is instructive to evaluate the fraction of high-energy neutrino alerts (Aartsen et al. 2017b; Blaufuss et al. 2019) that lead to likely associations with counterparts. If one further factors in the completeness of the catalog of potential counterparts, one can translate this fraction into a constraint on the contribution of the specific source class to the total neutrino flux. Below, we examine blazars and TDEs that have been identified so far in association with IceCube's neutrino alerts.

We first consider blazars that were found in association with the $N_{\rm alert} \sim 60$ alerts[6][7] sent to the community by IceCube so far: besides the well-known TXS0506+056 (Aartsen et al. 2018b), more recently PKS 1502+106—another exceptionally bright blazar—was identified in coincident with a well-localized neutrino track (Taboada & Stein 2019). Other claimed associations are less significant (e.g., GB6 J1040+0617, Garrappa et al. 2019) and/or have not been found in associations with alerts (PKS 1424-41; Kadler et al. 2016),

[6] https://gcn.gsfc.nasa.gov/amon_hese_events.html.
[7] https://gcn.gsfc.nasa.gov/amon_ehe_events.html.

and since we do not consider backgrounds here, they are not counted in this simple exercise. We hence count two detections, $N_{\rm det} = 2$. We take into account that roughly half of IceCube's alerts are estimated to be of astrophysical origin (signalness[8] $s \approx 0.5$). In addition, based on their gamma-ray flux, we assume that a fraction $f \sim 0.7$ of the high-energy neutrino flux from this source type are from electromagnetically resolved blazars (Ackermann et al. 2016). With these quantities, we can estimate the fraction of cosmic, high-energy neutrinos due to a blazar population: $N_{\rm det}/N_{\rm alert}/f/s = 0.10$.

Likewise for TDEs, Stein et al. (2021) associated one TDE ($N_{\rm det} = 1$) from a search of alerts ($N_{\rm alerts} = 9$). We estimate TDEs' completeness factor to be $f = 0.5$, which assumes that TDEs can be detected electromagnetically out to $\sim$1 Gpc. These numbers translate to a fraction of the diffuse neutrino flux due to a population of TDEs of $N_{\rm det}/N_{\rm alert}/f/s = 0.45$.

These initial estimates come with significant caveats, e.g., they do not take into account the significance of the observations, and moreover are not generalizable to observations that are not based on single-neutrino coincidences. Nevertheless, they are illustrative of a key point, namely the importance of the completeness of the catalog of counterparts in extrapolating the flux to a full population of sources.

3. Simple Model

In order to characterize the role of different population properties in connecting detections with the estimated contribution to the overall cosmic neutrino flux, we consider the following simple model. We separately consider continuous neutrino sources that are detected through time-integrated searches, and searches that identify sources via the detection of a single high-energy neutrino. Similar computations of converting resolved sources to overall cosmic flux can be found in the literature; see, e.g., Lipari (2008), Silvestri & Barwick (2010), Ahlers & Halzen (2014), and Murase & Waxman (2016).

3.1. Time-integrated Detection

Time-integrated searches are particularly relevant for continuous sources with high number densities where the detection of multiple neutrinos is necessary to claim detection. Let $F_{\nu,0}$ be the neutrino threshold above which such a time-integrated search is able to identify a neutrino flux. For simplicity, we neglect any dependence on the sources' neutrino spectrum and sky location.

Let sources within a given source type be uniformly distributed in the local universe with number density ρ. Let each source have unknown identical neutrino luminosity L_ν. The maximum distance $r_{\rm max}$ within which these sources can be detected is

$$r_{\rm max} = \sqrt{\frac{L_\nu}{4\pi F_{\nu,0}}}. \quad (1)$$

Within this distance, the expected number of sources is

$$\langle N_{\rm det} \rangle = \frac{4}{3}\pi r_{\rm max}^3 \, \rho. \quad (2)$$

We will consider the number $N_{\rm det}$ of detected sources to be the best estimate of the expected number of detections, i.e., $\langle N_{\rm det} \rangle = N_{\rm det}$. With this, the expected neutrino flux from the considered source type within $r_{\rm max}$ is

$$F_{\nu,r} = \int_0^{r_{\rm max}} dr 4\pi r^2 \rho \frac{L_\nu}{4\pi r^2} = \rho L_\nu r_{\rm max} = 3F_{\nu,0}N_{\rm det}, \quad (3)$$

where we made use of Equations (1) and (2) to change variables.

Let $f_{\rm r}(r_{\rm max})$ be the fraction of the total neutrino flux from a given source type that comes from sources within distance $r_{\rm max}$. For distances that are not too large, we approximate the dependence of $f_{\rm r}$ on $r_{\rm max}$ to be linear, i.e., $f_{\rm r}(r_{\rm max}) = f_0 \, r_{\rm max}$, where f_0 is a source-type-dependent constant. To compute f_0, we need to integrate the neutrino flux from the entire source population accounting for cosmic evolution (Bartos et al. 2017). With this, we can express the overall flux expected from the considered source type as (see also Murase et al. 2018, 2012)

$$F_{\nu,\rm tot}^{\rm (int)} = \frac{F_{\nu,r}(r_{\rm max})}{f_{\rm r}(r_{\rm max})} = \frac{3F_{\nu,0}N_{\rm det}}{f_0 \, r_{\rm max}} \approx 5F_{\nu,0}f_0^{-1}N_{\rm det}^{2/3}\rho^{1/3}, \quad (4)$$

where the superscript "(int)" refers to time-integrated detection. We see that, for the same number of detections, the corresponding flux can be very different due to its dependence on ρ, which can vary by orders of magnitude between sources.

3.2. Single-neutrino Detection

For rare and/or transient sources, a single high-energy neutrino can be sufficient to claim detection. Let $F_{\nu,1}$ be the source flux for which the *expected* number of detected neutrinos is 1 during the observing period $T_{\rm obs}$. For transient sources with duration τ, the corresponding actual source flux is $T_{\rm obs}/\tau$ times higher.

Let sources within a given source type be uniformly distributed in the local universe with number density ρ. Let each source have identical neutrino luminosity L_ν. For transient sources, we will adopt the same notation defining $\rho = \mathcal{R}T_{\rm obs}$ with source rate density $\mathcal{R}$, and $L_\nu = E_\nu T_{\rm obs}^{-1}$ with E_ν total energy radiated in high-energy neutrinos.

A single neutrino can only lead to discovery if it is directionally (and for transients, temporally) coincident with a source candidate. A single neutrino can be detected with nonvanishing probability even from distant sources. Therefore, single-neutrino searches will not be limited by a distance threshold for detection as in the time-integrated case. Instead, a solution is that the number of source candidates considered in the search is capped in order to limit the search's trial factor. Source candidates will be selected for a search such that those expected to have the highest neutrino flux at Earth are included. If all sources produce the same neutrino flux, then the closest sources are selected. If we limit the source candidates in a search to the number $N_{\rm max}$, then this corresponds to an effective

[8] IceCube neutrino alerts have an assigned quantity called signalness, defined as the probability that the neutrino signal came from an astrophysical, as opposed to an atmospheric source, based on the neutrino energy, sky location, and time of arrival, but without accounting for information from electromagnetic observations Blaufuss et al. (2019).

maximum search distance of

$$r_{\rm max} = \left(\frac{3N_{\rm max}}{4\pi\rho}\right)^{1/3}. \quad (5)$$

The expected number of detected sources within this distance is

$$\langle N_{\rm det}\rangle = \int_0^{r_{\rm max}} dr 4\pi r^2 \rho \frac{L_\nu}{4\pi r^2} F_{\nu,1}^{-1} = \rho L_\nu r_{\rm max} F_{\nu,1}^{-1}, \quad (6)$$

where we assumed that the expected number of detected neutrinos from a single source is $\ll 1$.

We will consider the number $N_{\rm det}$ of detected sources to be the best estimate of the expected number of detections, i.e., $\langle N_{\rm det}\rangle = N_{\rm det}$. With this, the expected neutrino flux from the considered source type within $r_{\rm max}$ is

$$F_{\nu,r}(r_{\rm max}) = \int_0^{r_{\rm max}} dr 4\pi r^2 \rho \frac{L_\nu}{4\pi r^2} = \rho L_\nu r_{\rm max} = F_{\nu,1} N_{\rm det}, \quad (7)$$

where we made use of Equation (6) to change variables.

Similarly to the previous section, we introduce the fraction $f_{\rm r}(r_{\rm max}) = f_0 r_{\rm max}$ of the total neutrino flux from a given source type that comes from sources within distance $r_{\rm max}$. With this, we can express the overall flux expected from the considered source type as

$$F_{\nu,\rm tot}^{\rm (single)} = \frac{F_{\nu,r}(r_{\rm max})}{f_{\rm r}(r_{\rm max})} = \frac{F_{\nu,1} N_{\rm det}}{f_0 r_{\rm max}} \approx \frac{1.6 F_{\nu,1} N_{\rm det} \rho^{1/3}}{f_0 N_{\rm max}^{1/3}}, \quad (8)$$

where the superscript "(single)" refers to single-neutrino detection. This formula is very similar to the one we obtained for time-integrated searches (see Equation (4)), and shows that the number density (or rate density) of sources can substantially alter the expected contribution from a source type.

3.3. Estimated Contribution Based on Simple Model

We now estimate the contribution of different detected source types to the cosmic neutrino flux. We additionally consider sources that have so far been undetected, to gauge how strong constraint their nondetection represents to their contribution to the overall flux. In this section, we made no constraint on the combined contribution of the considered source type, i.e., it is interesting that their total contribution is less than, but comparable to, the total IceCube flux.

3.4. Flux Fraction

First, we computed f_0 for different source populations, which is necessary to estimate their total flux. We considered (non-jetted) AGNs, tidal disruption events (TDEs), and for comparison, populations that follow the cosmic star formation rate. Our results are shown in Figure 1. For AGNs, we adopted their number density for bolometric luminosity $>10^{43}\,{\rm erg\,s^{-1}}$ from Lacy et al. (2015). For TDEs, we adopted their cosmic density evolution from Sun et al. (2015), while we adopted the cosmic star formation rate from Li (2008).

3.4.1. Blazars

We adopted the density $\rho_{\rm blazar} = 10^{-9}\,{\rm Mpc^{-3}}$ corresponding to a high-luminosity class of blazars called flat-spectrum radio quasars (FSRQs; Murase & Waxman 2016). With this choice, we assume that a subclass of blazars, FSRQs, are mainly responsible for neutrino emission from this class. We used

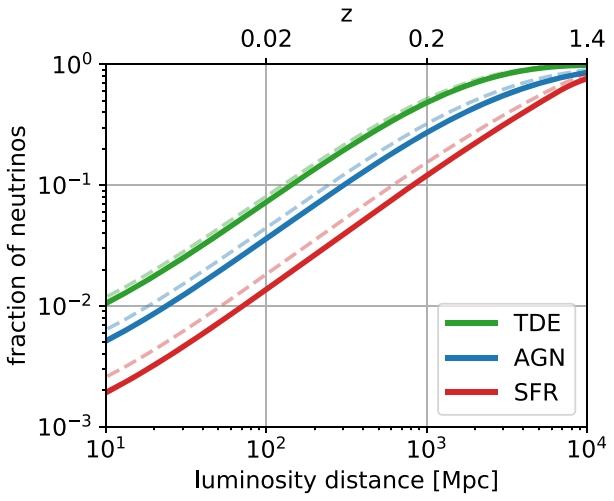

Figure 1. Fraction of detected high-energy neutrinos in IceCube expected from sources closer than luminosity distance $d_{\rm L}$ as a function of $d_{\rm L}$. Shown are results for AGNs/blazars, TDEs, and source populations that track the cosmic star formation rate (SFR; see legend). Solid lines show results for assumed neutrino spectral density $dN/dE \propto E^{-2.5}$. For comparison, we show for $dN/dE \propto E^{-3}$ (dashed lines).

$N_{\rm det} = 3$ and $T_{\rm obs} = 5\,{\rm yr}$. The choice of $T_{\rm obs}$ reflects the duration since IceCube began real-time alerts. We considered blazars to be detectable with single-neutrino searches. We adopted $\mathcal{F}_{\nu,1} = 4\times10^{-10}\,{\rm erg\,cm^{-2}\,s^{-1}}(1\,{\rm yr}/T_{\rm obs})$, where we assumed a neutrino spectral index of 2.5 and neutrino energy range $\varepsilon_\nu \in [100\,{\rm GeV},\ 100\,{\rm PeV}]$.[9] We further adopted $f_0 = 5\times10^{-4}\,{\rm Mpc^{-1}}$ (see Figure 1; we considered the same fraction for AGNs and blazars) and $N_{\rm max} = 100$ (see Aartsen et al. 2020c). With these parameters, we obtained $F_{\nu,\rm tot}^{\rm (blazar)} = 3\times10^{-9}\,{\rm erg\,cm^{-2}\,s^{-1}}$.

3.4.2. AGNs

For AGNs, we used $N_{\rm det} = 1$ and $\rho_{\rm AGN} = 10^{-4}\,{\rm Mpc^{-3}}$. We considered AGNs to be detectable with a time-integrated search. We adopted $F_{\nu,0} = 2\times10^{-11}\,{\rm erg\,cm^{-2}\,s^{-1}}$, where we assumed a neutrino spectral index of 2.5 and energy range $\varepsilon_\nu \in [100{\rm GeV},\ 100{\rm PeV}]$. We further adopted $f_0 = 3\times10^{-4}\,{\rm Mpc^{-1}}$.

With these parameters, we obtained $F_{\nu,\rm tot}^{\rm (AGN)} = 2\times10^{-8}\,{\rm erg\,cm^{-2}\,s^{-1}}$.

3.4.3. TDEs

For TDEs, we used $N_{\rm det} = 1$ and $\rho_{\rm TDE} = \mathcal{R}_{\rm TDE} T_{\rm obs} = 10^{-9.5}\,{\rm Mpc^{-3}}$, where we assumed $T_{\rm obs} = 5\,{\rm yr}$. We considered TDEs to be detectable with single-neutrino searches. We adopted $\mathcal{F}_{\nu,1} = 4\times10^{-10}\,{\rm erg\,cm^{-2}\,s^{-1}}(1\,{\rm yr}/T_{\rm obs})$, assuming a neutrino spectral index of 2.5 and neutrino energy range $\varepsilon_\nu \in [100{\rm GeV},\ 100{\rm PeV}]$. We adopted $f_0 = 9\times10^{-4}\,{\rm Mpc^{-1}}$.

In order to determine $N_{\rm max}$, we set the maximum detectable distance of TDEs to be $r_{\rm max,TDE} = 1\,{\rm Gpc}$ given the distance range of past identified TDEs (van Velzen et al. 2021). We assumed that electromagnetic follow-up of $\gtrsim 100$ TeV

[9] Here, we used the flux corresponding to an expected number of 1 detected neutrino in the $\varepsilon_\nu \in [100\,{\rm TeV},\ 100\,{\rm PeV}]$ from IceCube Collaboration (2016). We then extrapolated this flux to the energy range $\varepsilon_\nu \in [100\,{\rm GeV},\ 100\,{\rm PeV}]$ to make it compatible with the flux from the time-integrated search. We adopted a neutrino spectral index of 2.5 for the extrapolation.

neutrinos could identify every TDE within $r_{\rm max,TDE}$. We set $N_{\rm max} = 4/3\pi r_{\rm max,TDE}^3 \rho_{\rm TDE} \approx 1$.

With these parameters, we obtained $F_{\nu,\rm tot}^{\rm (TDE)} = 1.6 \times 10^{-8}$ erg cm^{-2} s^{-1}.

3.4.4. Gamma-ray Bursts

While no significant neutrino emission has been associated with gamma-ray bursts (GRBs), here we considered the corresponding total flux from GRBs assuming $N_{\rm det} = 2.3$, which is the 90% confidence level upper limit corresponding to no detections. This can give us a picture of the total flux contribution that is consistent with the lack of association. We adopted a local density of $\rho_{\rm GRB} = \mathcal{R}_{\rm GRB} T_{\rm obs} = 10^{-8}\,{\rm Mpc}^{-3}$ where we assumed $T_{\rm obs} = 10$ yr (Wanderman & Piran 2010). We considered GRBs to be detectable with single-neutrino searches.

Given the short duration and rarity of GRBs, and their easy observability with all-sky gamma-ray detectors, single-neutrino searches can consider neutrinos below the 100 TeV limit used for other single-neutrino searches. Adopting a threshold of 1 TeV and a neutrino spectral index of 3, we consider a threshold flux $\mathcal{F}_{\nu,1} = 4 \times 10^{-9}$ erg cm^{-2} s^{-1}(1 yr/$T_{\rm obs}$), i.e., 100 times lower than for an energy threshold of 100 TeV.

We adopted $f_0 = 2 \times 10^{-4}\,{\rm Mpc}^{-1}$, similar to the fraction expected for a population tracing the star formation rate. We took $N_{\rm max} = 1000$, comparable to the total number of detected GRBs.

With these parameters, we obtained $F_{\nu,\rm tot}^{\rm (GRB)} \lesssim 10^{-9}$ erg cm^{-2} s^{-1}. We conclude that the lack of detection presents a strong constraint on the GRB contribution to the total cosmic neutrino flux: their contribution is <1%. This limit is consistent with constraints from searches by IceCube for neutrinos coincident with GRBs (Aartsen et al. 2017a).

3.4.5. Core-collapse Supernovae

No significant neutrino emission has been associated with supernovae. Here, we considered the corresponding total flux from core-collapse supernovae assuming $N_{\rm det} = 2.3$ to characterize the limit this lack of detection represents.

We adopted a core-collapse supernova rate density of $\sim 10^{-4}\,{\rm Mpc}^{-3}{\rm yr}^{-1}$ (Taylor et al. 2014), and assumed that neutrino emission is significant for a duration of $T_{\rm obs} = 10$ yr. With this, we obtain an effective density $\rho_{\rm SN} = 10^{-3}\,{\rm Mpc}^{-3}$. We considered supernovae to be detectable with time-integrated searches.

We adopted $F_{\nu,0} = 2 \times 10^{-11}$ erg cm^{-2} s^{-1}, where we assumed a neutrino spectral index of 2.5 and energy range $\varepsilon_\nu \in [100\,{\rm GeV},\ 100\,{\rm PeV}]$ (see also Murase 2018; Murase & Ioka 2013). We further adopted $f_0 = 1.5 \times 10^{-4}\ {\rm Mpc}^{-1}$, assuming that the supernova rate traces the star formation rate.

With these parameters, we obtained $F_{\nu,\rm tot}^{\rm (CCSN)} \lesssim 10^{-7}$ erg cm^{-2} s^{-1}, i.e., greater than IceCube's overall flux. We therefore conclude that the lack of observation does not present a meaningful constraint on the contribution of supernovae to the total cosmic neutrino flux.

3.4.6. Starburst Galaxies

Starburst galaxies have been proposed as a major contributor to the cosmic high-energy neutrino flux (Loeb & Waxman 2006; Anchordoqui et al. 2014; Tamborra et al. 2014; Murase & Waxman 2016; Bechtol et al. 2017). No direct association has been made so far. We adopted an effective number density of $\rho_{\rm starburst} = 10^{-5}\,{\rm Mpc}^{-3}$ (Murase & Waxman 2016); $F_{\nu,0} = 2 \times 10^{-11}$ erg cm^{-2} s^{-1}, where we assumed a neutrino spectral index of 2.5 and energy range $\varepsilon_\nu \in [100\,{\rm GeV},\ 100\,{\rm PeV}]$; and $f_0 = 1.5 \times 10^{-4}\,{\rm Mpc}^{-1}$, assuming that the starburst galaxies trace the star formation rate.

We further considered $N_{\rm det} = 2.3$ to characterize the limit that the lack of detection represents. Using Equation (4), we obtained $F_{\nu,\rm tot}^{\rm (starburst)} \lesssim 2.5 \times 10^{-8}$ erg cm^{-2} s^{-1}, limiting the starburst contribution to $\lesssim 40\%$ of the IceCube flux. A higher effective number density for starburst galaxies would correspond to an even less stringent constraint.

4. Full Bayesian Model

We now turn to a more detailed derivation of the expected neutrino flux from different source populations where we take into account the cosmic evolution of sources and the statistical uncertainty of the number of detections.

4.1. Probability Density of the Expected Number of Detections

Assume we have a set of $N_{\rm tot}$ detection candidates for source type S. Each candidate is either from the astrophysical source of interest or from the background. For our purposes here, astrophysical neutrinos from unassociated sources are counted as background. Candidate i has a set of reconstructed parameters denoted with $\boldsymbol{x}_i$. The set of reconstructed parameters for all candidates is denoted with $\boldsymbol{x} = \{\boldsymbol{x}_1, \boldsymbol{x}_2 \ldots \boldsymbol{x}_{\rm N_{tot}}\}$.

Let $p(\boldsymbol{x}_i|S)$ and $p(\boldsymbol{x}_i|B)$ be the probability densities of observing $\boldsymbol{x}_i$ from an astrophysical source of type S and from the background, respectively. We compute the probability density of the expected number of detected events, denoted with $N_{\rm det}$ as (Farr et al. 2015) (note the similarity to Equation (7) in Braun et al. 2008):

$$p(N_{\rm det}|\boldsymbol{x}) \propto \int dN_{\rm B} \prod_{i=1}^{N_{\rm tot}} [N_{\rm det} p(\boldsymbol{x}_i|S) + N_{\rm B} p(\boldsymbol{x}_i|B)] \times e^{-(N_{\rm det}+N_{\rm B})} \frac{\pi(N_{\rm det})}{\sqrt{N_{\rm B}}}, \quad (9)$$

where $N_{\rm B}$ is the expected number of detected background events, which we marginalize over. We used the Poisson Jeffreys prior for $N_{\rm B}$. We define the prior probability density $\pi(N_{\rm det})$ of $N_{\rm det}$ implicitly by assuming that the prior probability density of the total flux from a given source type is uniformly distributed between 0 and IceCube's measured cosmic neutrino flux minus the flux of the other sources. Therefore, we will have a three-dimensional prior probability density for the three sources considered below, with uniform probability density and with the boundary condition that the sum of the total flux from the three sources cannot exceed IceCube's measured flux.

4.2. Computing the Neutrino Luminosity of Individual Sources

If we know the expected number of detected sources, we can compute the related neutrino luminosity of individual sources. This computation, however, also depends on the luminosity's probability density.

Here, we will assume that the neutrino luminosity L_ν of a source depends on its electromagnetic luminosity L_γ (see Section 5 for model-dependent assumptions on L_γ). For simplicity, we will assume that $L_\nu = \alpha_{\gamma\nu} L_\gamma$ with unknown $\alpha_{\gamma\nu}$ constant. We further assume that we know the number

density $\rho(z, L_\gamma)$ of a continuous source type as a function of redshift z and L_γ.

With this, we can compute the expected number of detections (see also Murase & Waxman 2016):

$$N_{\rm S,cont.} = \int dz dL_\nu \frac{4\pi c}{H(z)} \frac{d_{\rm L}(z)^2}{(1+z)^2} \rho(z, \frac{L_\nu}{\alpha_{\gamma\nu}}) p_{\rm det}(z, L_\nu). \quad (10)$$

Here, $d_{\rm L}$ is the luminosity distance and $p_{\rm det}(z, L_\nu)$ is the probability that a source with luminosity L_ν at redshift z will be detected. We can compute the expected detection rate for transient sources as well, where we also need to take into account time dilation, obtaining

$$N_{\rm S,trans.} = T_{\rm obs} \int dz dE_\nu \frac{4\pi c}{H(z)} \frac{d_{\rm L}(z)^2}{(1+z)^3} \times \mathcal{R}(z, \frac{E_\nu}{\alpha_{\gamma\nu}}) p_{\rm det}(z, E_\nu). \quad (11)$$

Here, $T_{\rm obs}$ is the duration of observation, $\mathcal{R}(z, E_\gamma)$ is the comoving rate density, and $E_\gamma = \alpha_{\gamma\nu} E_\nu$ is the radiated electromagnetic energy.

We can then compute the unknown $\alpha_{\gamma\nu}$ factor by equating the expected number of detections from Equations (10) or (11) with the expected number of detections from observations.

Note that, if we assumed that all sources have the same neutrino luminosity, then this step would not be needed and we could simply compute the overall neutrino flux from the number of detections from observations. However, this step enables the incorporation of the source luminosity distribution, which we can base on the observed γ luminosity distributions for the source types in question.

An interesting side product of this step is the determination of $\alpha_{\gamma\nu}$, i.e., the connection between the sources' gamma flux and expected neutrino flux given the number of detections. For blazars and AGNs discussed below, we obtain a characteristic conversion factor of $\alpha_{\gamma\nu}^{\rm blazar} \sim 5$ and $\alpha_{\gamma\nu}^{\rm AGN} \sim 0.04$. These characteristic values are obtained by assuming that the number of detections is the expected number (as considered in our "simple model"). It therefore appears that blazars are more efficient neutrino producers than AGNs.

4.3. Expected Total Flux at Earth

To obtain the expected total neutrino flux at Earth for a source type, we integrate over all sources in the universe. We also marginalize over the distribution of the expected number of detections from Equation (9). For continuous sources, we obtain

$$\mathcal{F}_{\nu,\rm S,cont.} = \int dN_{\rm det} dz dL_\nu d\theta \frac{c}{H(z)} \rho(z, L_\nu, N_{\rm det}) \times p_{\rm det}(z, L_\nu) \frac{L_\nu}{(1+z)^{2+\alpha}} p(N_{\rm det}|\boldsymbol{x}), \quad (12)$$

where α is the spectral index of the neutrino spectral density $dN_\nu/d\varepsilon_\nu \propto \varepsilon^{-\alpha}$, and we expressed ρ as a function of $N_{\rm det}$ and L_ν. The latter takes into account that we do not know the density spectrum of L_ν but can determine it using the density spectrum of L_γ and $N_{\rm det}$ and by assuming that $L_\nu \propto L_\gamma$. We can similarly compute the total flux at Earth for transients:

$$\mathcal{F}_{\nu,\rm S,trans.} = \int dN_{\rm det} dz dL_\nu d\theta \frac{c}{H(z)} \mathcal{R}(z, L_\nu, N_{\rm det}) \times p_{\rm det}(z, L_\nu) \frac{L_\nu}{(1+z)^{3+\alpha}} p(N_{\rm det}|\boldsymbol{x}). \quad (13)$$

5. Implementation

Here, we implement the general framework discussed above by considering available information from observations.

5.1. Source Parameter Probability Densities

We now turn to $p(\boldsymbol{x}_i|B)$ and $p(\boldsymbol{x}_i|S)$. We consider $\boldsymbol{x}_i = p_i$. The probability density of the p-value is naturally defined for the background distribution as uniform ($p(\boldsymbol{x}_i|B) = 1$). However, the signal distribution $p(\boldsymbol{x}_i|z_i, L_{\nu,i}S)$ cannot be determined without a specific astrophysical signal model and the data analysis framework used in the search. Instead, we adopt a "calibrated" ratio of the background and signal probability densities from Sellke et al. (2001):

$$\frac{p(\boldsymbol{x}_i|B)}{p(\boldsymbol{x}_i|S)} = -e\, p_i \ln(p_i) \quad (14)$$

for $p_i < 1/e$, where e is Euler's number. This ratio is a lower bound over a wide range of realistic p-value distributions for the signal hypothesis where the only assumption is that the density of p_i under the signal hypothesis should be decreasing in p_i. As this "calibrated" ratio is a lower bound, it may still be optimistic in terms of the flux contributions. Nevertheless, we consider this a reasonable "calibrated" estimate given the unknown signal hypothesis.

5.2. Detection Probability

For a given redshift and neutrino luminosity, the probability of detection depends on both the identification of the source through electromagnetic observations and on the detectability of the neutrino signal. Electromagnetic identification determines the completeness $\mathcal{C}(z, L_\gamma)$ of a source catalog, where L_γ is the electromagnetic luminosity of the source. We assumed here that neutrino luminosity is proportional to the electromagnetic luminosity of the source, i.e., $L_\gamma \propto L_\nu$

The detectability of the neutrino signal depends on multiple factors, including the neutrino flux and spectrum at Earth, detector sensitivity, and the number density of the source population. In the limit of rare sources, even a single neutrino will be sufficient to identify a source. In this case, detectability will be the probability that a single neutrino is recorded. To obtain this probability for a given source flux, we adopted the expected number of detected neutrinos for a given flux presented by IceCube Collaboration (2016). For a source spectrum $dN_\nu/d\varepsilon_\nu \propto \varepsilon_\nu^{-2.5}$, the flux density corresponding to an expected single detected neutrino is $1.2 \times 10^{-17}\,{\rm GeV}^{-1}\,{\rm cm}^{-2}\,{\rm s}^{-1}\,(\varepsilon_\nu/100\,{\rm TeV})^{-2.5}(T_{\rm obs}/1\,{\rm yr})^{-1}$.

For more common sources, detectability can be approximated with a flux threshold $\mathcal{F}_{\nu,\rm th}$ such that all those—and only those—sources with flux $\mathcal{F} \geqslant \mathcal{F}_{\nu,\rm th}$ are detected. Below, we adopt $\mathcal{F}_{\nu,\rm th}$ from IceCube's 10 yr, 90% confidence-level median sensitivity based on Aartsen et al. (2020c), integrated within [100 GeV, 100 PeV]. For E^{-3} and E^{-2} spectra, this sensitivity is $\mathcal{F}_{\nu,\rm th,3} = 2 \times 10^{-10}\,{\rm erg\,cm^{-2}\,s^{-1}}$ and $\mathcal{F}_{\nu,\rm th,2} = 10^{-11}$

Table 1
Astrophysical Sources with Associated Neutrino Emission Used in This Analysis

Name	Type	p	Ref.
NGC 1068	AGN	0.008	Aartsen et al. (2020c)
TXS 0506+056	blazar	0.001	Aartsen et al. (2018a)
PKS 1502+106	blazar	0.01	Taboada & Stein (2019)
PKS 1424-41	blazar	0.05	Kadler et al. (2016)
AT2019dsg	TDE	0.002	Stein et al. (2021)

Note. p is the p-value of the neutrino signal's association with the astrophysical source.

erg cm^{-2} s^{-1}, respectively. To obtain the sensitivity for an $E^{-2.5}$ spectrum, we consider the geometric mean of $\mathcal{F}_{\nu,\mathrm{th},3}$ and $\mathcal{F}_{\nu,\mathrm{th},2}$, obtaining $\mathcal{F}_{\nu,\mathrm{th},2.5} = 2 \times 10^{-11}$ erg cm^{-2} s^{-1}. These values are valid for the Northern Hemisphere. We account for the fact that IceCube is much more sensitive toward the Northern Hemisphere by introducing an effective factor-of-two reduction in source completeness.

To characterize the dependence of our results to these approximate sensitivity threshold, we can look at Equations (4) and (8), which show in the case of our simplified model that the results are linearly dependent on the thresholds. This can be somewhat mitigated in our full model by the overall constraint that the total flux is less than the IceCube flux.

5.3. Source Types

Here, we introduce the source properties used for the analysis.

5.3.1. Active Galactic Nuclei

One active galactic nucleus (AGN), NGC 1068, has been identified as a likely neutrino source at 2.9σ post-trial significance Aartsen et al. (2020c). We use this one detection, with p-value $p = 2 \times 10^{-3}$. We adopt the cosmic number density and luminosity function $\rho_{\mathrm{AGN}}(z, L_\gamma)$ for AGNs from the Spitzer mid-infrared AGN survey (Lacy et al. 2015), with threshold $L_\gamma \geqslant 10^{41}$ erg s^{-1}. We consider AGNs detected as neutrino sources if their neutrino flux is above the threshold $\mathcal{F}_{\nu,\mathrm{th}}$. This flux threshold is adopted based on the measured (90% C.L. median) sensitivity of IceCube's 10 yr search (Aartsen et al. 2020c). We use the typical sensitivity at the Northern Hemisphere given that IceCube is much more sensitive in this direction, and adopt a factor-of-two reduction in the completeness of the AGN catalog. For a source with neutrino spectral index 2, this corresponds to $\mathcal{F}_{\nu,\mathrm{th},2} = 6 \times 10^{-13}$ erg cm^{-2} s^{-1}, considering neutrino energies $\varepsilon_\nu \in [100\,\mathrm{GeV}, 100\,\mathrm{PeV}]$. For neutrino spectral index 3, we find $\mathcal{F}_{\nu,\mathrm{th},3} = 2 \times 10^{-10}$ erg cm^{-2} s^{-1}.

In the detection process, only a few AGNs have been used in neutrino searches, selected based on their γ-ray brightness (Aartsen et al. 2020c). This limitation ensured that the trial factor in the search remained low. We take this into account by limiting the completeness of our simulated catalog to the 10 brightest sources on the northern hemisphere, i.e., p_{det} is set to zero for sources with z and L_γ for which the electromagnetic flux at Earth is below a threshold (10^{-9} erg cm^{-2} s^{-1}) such that 10 sources are expected.

5.3.2. Blazars

For blazars, we consider three detections (see Table 1). We adopt the cosmic number density and radio luminosity function $\rho_{\mathrm{blazar}}(z, L_\gamma)$ for FSRQs from Mao et al. (2017), with threshold $L_\gamma \geqslant 10^{40}$ erg s^{-1}. We consider a blazar detected if a single extremely high-energy neutrino with energy above 100 TeV is detected from it. For a source with spectral index 2, one extremely high-energy neutrino is expected to be detected from a source in a random direction (IceCube Collaboration 2016) for a neutrino flux of $\mathcal{F}_{\nu,\mathrm{single},2} = 4 \times 10^{-10}$ erg cm^{-2} s^{-1}($1\,\mathrm{yr}/T_{\mathrm{obs}}$) in the neutrino energy range $\varepsilon_\nu \in [100\,\mathrm{TeV}, 100\,\mathrm{PeV}]$. For spectral index 3, we also have $\mathcal{F}_{\nu,\mathrm{single},3} = 4 \times 10^{-10}$ erg cm^{-2} s^{-1}($1\,\mathrm{yr}/T_{\mathrm{obs}}$).

Similarly to AGNs, we limit the number of blazars in our search catalog. IceCube's 10 yr catalog search included about 100 blazars (Aartsen et al. 2020c); we therefore adopt the same number here.

5.3.3. TDEs

The detection of one TDE, AT2019dsg, has been reported so far in Stein et al. (2021), which we include in this analysis. We adopt the cosmic rate density of TDEs from Sun et al. (2015), using a minimum TDE luminosity of $L_\gamma = 10^{44}$ erg s^{-1}. We consider the rate and evolution of all TDEs, i.e., we do not require the presence of TDE jets. For simplicity, we treat all TDEs as having identical neutrino luminosity and detectability.

Given the regular electromagnetic follow-up of very high-energy neutrinos released publicly by IceCube, we will consider the catalog of TDEs complete out to the distance they can be found through electromagnetic observations. Given the distance range of past identified TDEs (van Velzen et al. 2021), we set their detectable distance at $r_{\mathrm{max,TDE}} = 1$ Gpc.

We can compute the total fluence needed for the expected detection of a single neutrino analogously for blazars, but using fluence instead of flux. For a source with spectral index 2, we find a neutrino fluence of $\mathcal{S}_{\nu,\mathrm{single},2} = 0.1$ erg cm^{-2} in the neutrino energy range $\varepsilon_\nu \in [100\,\mathrm{TeV}, 100\,\mathrm{PeV}]$. For spectral index 3, we also have $\mathcal{S}_{\nu,\mathrm{single},3} = 0.1$ erg cm^{-2}.

6. Results

We computed the expected cosmic flux for AGNs, blazars, and TDEs using the above prescription. To understand the statistical uncertainty of our results, we obtained the flux probability densities for the three cases based on the probability density $p(N_{\mathrm{det}}|\boldsymbol{x})$ in Equation (9). Flux probability densities are computed similarly to Equation (12) for AGNs and blazars, and Equation (13) for TDEs, but without marginalization over N_{det}. Specifically, in this step we compute the probability densities $\partial\mathcal{F}_{\nu,\mathrm{S,cont.}}/\partial N_{\mathrm{det}}$ and $\partial\mathcal{F}_{\nu,\mathrm{S,trans.}}/\partial N_{\mathrm{det}}$ by carrying out the source simulation with different N_{det} values and then converting the array of results into a distribution.

The results are shown in Figure 2. We also list the expected values and 90% credible intervals in Table 2. We see that AGNs and TDEs have comparable expected fluxes, while the expected flux from blazars is about a factor of 3 lower than these. We also see that, due to the low number of detections so far, the expected flux has considerable uncertainties.

To obtain a pie chart of total fluxes, we look at the properties of the cosmic quasi-diffuse neutrino flux. IceCube detections are consistent with an astrophysical flux following a power-law distribution with spectral index of 2.53 ± 0.07 (Aartsen et al.

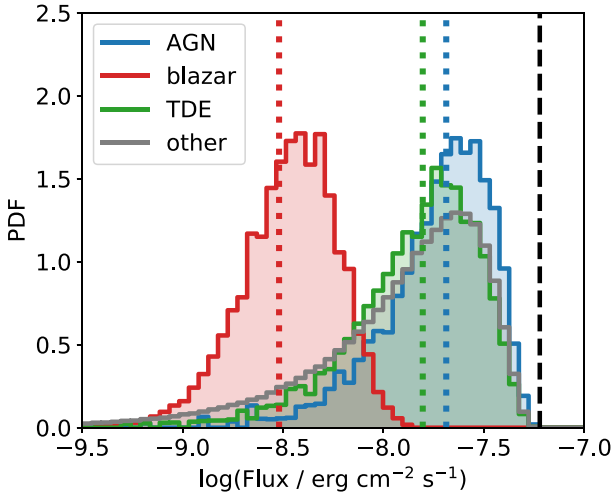

Figure 2. Probability density of total neutrino flux from AGNs, blazars, and TDEs based on IceCube's detected sources. For comparison, we show the total measured IceCube flux (vertical dashed black line; Aartsen et al. 2020), and the estimated flux for the three source types using our simple model (Section 3; vertical dotted lines). We assumed an $E^{-2.5}$ astrophysical neutrino spectrum (Aartsen et al. 2020).

Table 2
Estimated Cosmic Neutrino Flux as a Fraction of IceCube's Total Measured Flux (ϕ_{IC})

Type	Flux / ϕ_{IC}		
	Warm-up	Simple	Full
AGN		0.34	$0.36^{+0.31}_{-0.27}$
blazar	0.1	0.05	$0.06^{+0.06}_{-0.04}$
TDE	0.45	0.26	$0.29^{+0.30}_{-0.24}$
other			$0.28^{+0.38}_{-0.25}$
GRB		<0.01	
CCSN		<1	
starburst		<0.4	

Notes. Results are shown for the "warm-up" (Section 2), "simple" (Section 3), and "full" Bayesian (Section 4) models, for AGNs, blazars, and TDEs, and the total estimated flux from unknown source types. Error bars indicate 90% credible interval. For our "simple" model, we show upper limits for GRBs, indicating that nondetection presents a very strict constraint on their allowed contribution to the overall flux, due to their very low rate density; we also provide upper limits for core-collapse supernovae (CCSNe), showing that nondetection does not meaningfully constrain their contribution to the overall neutrino flux, due to their high rate density.

2020). Therefore, we consider a neutrino spectrum that scales as $E^{-2.5}$ with neutrino energy E. Our results would be similar to those presented below if we adopted a somewhat softer spectrum with E^{-3} that best fits the energy distribution of the highest-energy neutrinos (Abbasi et al. 2021).

We combine our results together for blazars, AGNs, and TDEs into a *pie chart* that shows the expected relative abundance of these three source types in the overall flux of high-energy neutrinos IceCube is detecting. The obtained pie chart is shown in Figure 3.

6.1. Expected Contribution from Other Source Types

Based on the probability densities of AGNs, blazars, and TDEs shown in Figure 2, we computed the expected contribution from other (unspecified) source types. For this,

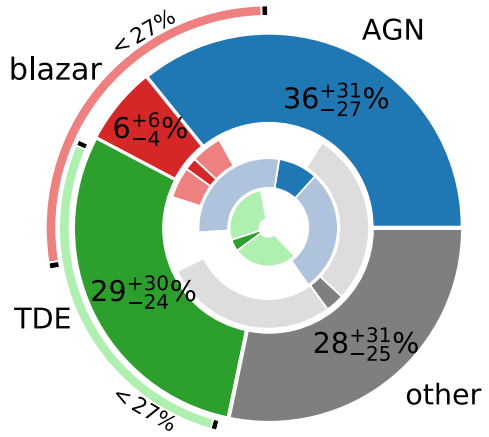

Figure 3. Pie chart of expected fraction of IceCube's neutrino flux from the three source types with directly associated neutrino detections, and the remaining flux from unknown sources (other). The main pie chart indicates the average expected fractional values, while the innermost charts indicate uncertainty by showing the minimum (dark) and maximum (light) extent of the fractional contributions allowed within the 90% credible regions. Outer thin slices further show independent observational constraints from stacking analyses for TDEs (Stein 2019) and blazars (Aartsen et al. 2017) that limit their contributions to <27% each at 90% confidence level.

we considered the AGN, blazar, and TDE probability densities to be independent and computed the probability density of their combined neutrino flux, with the boundary condition that the total cannot exceed IceCube's measured total flux. We found that the unknown sources represent at least 10% (1%) of IceCube's total flux with 80% (98%) probability. This fraction could be even higher given our (upper bound) estimation of the probability density ratio in Equation (14).

We note that this computation only accounts for the observed associations. It does not take into account independent source constraints or theoretically expected source energetics (Murase & Fukugita 2019) or emission efficiencies (Murase et al. 2020a). It is therefore interesting to compare our results with alternative expectations, which are largely consistent with our results within uncertainties.

7. Independent Observational Limits

While the present work computes fractional source contributions from associated events, source contribution limits have been previously derived through independent observing strategies.

A main strategy is to use the nondetection of very high-energy neutrino multiplets to constrain the flux of different source types (Kowalski 2015; Murase & Waxman 2016; Capel et al. 2020). The lack of such multiplets particularly limits transients, such as GRBs and TDEs, and rare source types, such as blazars. These source types are excluded as the dominant sources of the observed quasi-diffuse neutrino flux.

A stacking analysis found that TDEs cannot contribute more than 27% of the total diffuse astrophysical neutrino flux at 90% confidence level (Stein 2019).

The contribution of known blazars (those in Fermi's second catalog) to the total neutrino flux within 10 TeV and 2 PeV was limited by a stacking search to less than 27%, assuming a neutrino spectrum with index −2.5 (Aartsen et al. 2017).

Stacked searches have also been carried out for Type Ibc core-collapse supernovae (Esmaili & Murase 2018; Senno et al.

2018), but these do not rule out these sources as major contributors to the IceCube flux.

8. Conclusion

We computed the expected total high-energy neutrino flux at Earth from AGNs, blazars, and TDEs based on the associations of individual sources with astrophysical neutrinos detected by IceCube, IceCube's sensitivity, and the astrophysical properties and distributions of the three source types. We first carried out a simple derivation of the expected neutrino flux in order to demonstrate how the results scale with the properties of the detections, IceCube, and the sources. We then carried out a more detailed derivation that accounts for the statistical uncertainty of the detection process, varying neutrino luminosity within a source type, and the cosmic evolution of source densities and properties. Our conclusions are as follows:

1. Despite having detected more blazars with neutrinos than AGNs or TDEs, blazars are expected to be the smallest contributor to the cosmic neutrino flux. We found their contribution to be $3.9^{+3.7}_{-2.6} \times 10^{-9}$ erg s^{-1} cm^{-2} (error bars indicate 90% credible interval), or a contribution that is $< 11\%$ of the total quasi-diffuse neutrino flux detected by IceCube (at 90% credible level). This relatively small contribution is due to the fact that blazars are rare, making them much easier to identify through multi-messenger searches than a more common source type with similar total flux contribution. Significant contribution from low-luminosity blazars, nevertheless, could increase their fractional contribution (Palladino et al. 2019).
2. AGNs and TDEs represent similar overall contributions. We estimated the AGN flux to be $2.1^{+1.8}_{-1.6} \times 10^{-8}$ erg s^{-1} cm^{-2}, while for TDEs the estimated flux is $1.8^{+1.8}_{-1.4} \times 10^{-8}$ erg s^{-1} cm^{-2}. Either AGNs or TDEs could be the majority source of cosmic high-energy neutrinos. Their most likely contribution is about $1/3^{\rm rd}$ of the total flux for each.
3. One or more as-yet unidentified source types also likely contribute to the overall flux. We estimate their contribution to be $1.7^{+2.3}_{-1.5} \times 10^{-8}$ erg s^{-1} cm^{-2}.

The above results only accounted for information in source types with neutrino associations, i.e., our pie chart does not consider the breakdown of "other" source types, or more detailed prior theoretical expectations from promising source types such as starburst galaxies, galaxy clusters, or supernovae. We also do not fold in information from observational limits from stacked or other searches. Further sources of uncertainty include the assumed neutrino spectrum, which may have a different, and possibly non-power-law, spectrum for different source types (Palladino 2018). Despite these limitations, our results are broadly consistent with other observational and theoretical expectations within uncertainties.

The diversity of neutrino sources that apparently contribute to the diffuse flux and the further possibility of unidentified classes of neutrino sources that remained hidden so far makes future observations, and next-generation neutrino observatories such as IceCube-Gen2 (Aartsen et al. 2021) or KM3NeT (Adrián-Martínez et al. 2016), particularly interesting. The discovery of more AGNs, blazars, and TDEs, and the better resolution of the astrophysical high-energy neutrino spectrum, will also be key in enabling the characterization of unidentified source types even if they remain undetected through electromagnetic observations.

The authors thank Cecilia Lunardini, Kohta Murase, Foteini Oikonomou, Christopher Wiebusch, and Walter Winter for their valuable suggestions. The authors are grateful for the generous support of the University of Florida, DESY, and Columbia University in the City of New York. I.B. acknowledges the support of the National Science Foundation under grant PHY-1911796, and the Alfred P. Sloan Foundation.

ORCID iDs

I. Bartos https://orcid.org/0000-0001-5607-3637
D. Veske https://orcid.org/0000-0003-4225-0895
M. Kowalski https://orcid.org/0000-0001-8150-6561
Z. Márka https://orcid.org/0000-0003-1306-5260
S. Márka https://orcid.org/0000-0002-3957-1324

References

Aartsen, M., Abbasi, R., Abdou, Y., et al. 2013, Sci, 342, 1242856
Aartsen, M. G., Abbasi, R., Ackermann, M., et al. 2021, JPhG, 48, 060501
Aartsen, M. G., Abraham, K., Ackermann, M., et al. 2016, ApJ, 833, 3
Aartsen, M. G., Abraham, K., Ackermann, M., et al. 2017, ApJ, 835, 45
Aartsen, M. G., Ackermann, M., Adams, J., et al. 2014, PhRvL, 113, 101101
Aartsen, M. G., Ackermann, M., Adams, J., et al. 2017a, ApJ, 843, 112
Aartsen, M. G., Ackermann, M., Adams, J., et al. 2017b, APh, 92, 30
Aartsen, M. G., Ackermann, M., Adams, J., et al. 2018a, Sci, 361, eaat1378
Aartsen, M. G., Ackermann, M., Adams, J., et al. 2018b, Sci, 361, 147
Aartsen, M. G., Ackermann, M., Adams, J., et al. 2020, arXiv:2001.09520
Aartsen, M. G., Ackermann, M., Adams, J., et al. 2020c, PhRvL, 124, 051103
Abbasi, R., Abdou, Y., Abu-Zayyad, T., et al. 2012, Natur, 484, 351
Abbasi, R., Ackermann, M., Adams, J., et al. 2021, PhRvD, 104, 022002
Ackermann, M., Ajello, M., Albert, A., et al. 2016, PhRvL, 116, 151105
Adrián-Martínez, S., Ageron, M., Aharonian, F., et al. 2016, JPhG, 43, 084001
Ahlers, M., & Halzen, F. 2014, PhRvD, 90, 043005
Anchordoqui, L. A., Paul, T. C., da Silva, L. H. M., Torres, D. F., & Vlcek, B. J. 2014, PhRvD, 89, 127304
Bartos, I., Ahrens, M., Finley, C., & Márka, S. 2017, PhRvD, 96, 023003
Bechtol, K., Ahlers, M., Di Mauro, M., Ajello, M., & Vandenbroucke, J. 2017, ApJ, 836, 47
Blaufuss, E., Kintscher, T., Lu, L., & Tung, C. F. 2019, ICRC, 36, 1021
Braun, J., Dumm, J., De Palma, F., et al. 2008, APh, 29, 299
Capel, F., Mortlock, D. J., & Finley, C. 2020, PhRvD, 101, 123017
Esmaili, A., & Murase, K. 2018, JCAP, 2018, 008
Farr, W. M., Gair, J. R., Mandel, I., & Cutler, C. 2015, PhRvD, 91, 023005
Garrappa, S., Buson, S., Franckowiak, A., et al. 2019, ApJ, 880, 103
Guépin, C., Kotera, K., Barausse, E., Fang, K., & Murase, K. 2018, A&A, 616, A179
IceCube Collaboration 2016, Summary of the EHE Online Alert, NASA
Kadler, M., Krauß, F., Mannheim, K., et al. 2016, NatPh, 12, 807
Kowalski, M. 2015, JPhCS, 632, 012039
Kun, E., Bartos, I., Tjus, J. B., et al. 2021, ApJL, 911, L18
Lacy, M., Ridgway, S. E., Sajina, A., et al. 2015, ApJ, 802, 102
Li, L.-X. 2008, MNRAS, 388, 1487
Lipari, P. 2008, PhRvD, 78, 083011
Loeb, A., & Waxman, E. 2006, JCAP, 2006, 003
Mao, P., Urry, C. M., Marchesini, E., et al. 2017, ApJ, 842, 87
Murase, K. 2018, PhRvD, 97, 081301
Murase, K., Beacom, J. F., & Takami, H. 2012, JCAP, 2012, 030
Murase, K., & Fukugita, M. 2019, PhRvD, 99, 063012
Murase, K., & Ioka, K. 2013, PhRvL, 111, 121102
Murase, K., Kimura, S. S., & Mészáros, P. 2020a, PhRvL, 125, 011101
Murase, K., Kimura, S. S., Zhang, B. T., Oikonomou, F., & Petropoulou, M. 2020b, ApJ, 902, 108
Murase, K., Oikonomou, F., & Petropoulou, M. 2018, ApJ, 865, 124
Murase, K., & Waxman, E. 2016, PhRvD, 94, 103006
Palladino, A. 2018, in XXVIII Int. Conf. Neutrino Phys. Astrophys. (Heidelberg: MPI), 84
Palladino, A., Rodrigues, X., Gao, S., & Winter, W. 2019, ApJ, 871, 41
Sellke, T., Bayarri, M. J., & Berger, J. O. 2001, Am. Stat., 55, 62
Senno, N., Murase, K., & Mészáros, P. 2017, ApJ, 838, 3

Senno, N., Murase, K., & Mészáros, P. 2018, JCAP, 81, 023001
Silvestri, A., & Barwick, S. W. 2010, PhRvD, 81, 023001
Stein, R. 2019, ICRC, 36, 1016
Stein, R., Velzen, S. v., Kowalski, M., et al. 2021, NatAs, 5, 510
Sun, H., Zhang, B., & Li, Z. 2015, ApJ, 812, 33
Taboada, I., & Stein, R. 2019, ATel, 12967, 1
Tamborra, I., Ando, S., & Murase, K. 2014, JCAP, 2014, 043
Taylor, M., Cinabro, D., Dilday, B., et al. 2014, ApJ, 792, 135
van Velzen, S., Gezari, S., Hammerstein, E., et al. 2021, ApJ, 908, 4
Wanderman, D., & Piran, T. 2010, MNRAS, 406, 1944
Yuan, C., Murase, K., & Mészáros, P. 2020, ApJ, 890, 25